Nanocomposites and Alloys Based on Porous Silicon Filled with Metals and Semiconductors

Nikita Grevtsov*, Uliana Lopato*, Alexey Dolgyi*, Eugene Chubenko*, Vitaly Bondarenko*, A. Smirnov*, A. Stsiapanau*, A. Dronov**, I. Gavrilin**, S. Gavrilov*

Belarusian State Uni. of Informatics and Radioelectronics, Minsk, Belarus

****National Research Uni. of Electronic Tech., Zelenograd, Moscow, Russia**

Abstract

A variety of micro- and nanocomposite materials based on electrochemically-acquired porous silicon are produced and evaluated in terms of their applicability to display technology. It is shown that porous silicon provides a versatile and well-adjustable template for filling with other materials, which can outright change its electrophysical parameters. While, in terms of display applications, porous silicon layers are mostly prominent for their photoluminescence not akin to monocrystalline silicon, this property can be additionally enhanced by employing a variety of electrochemical techniques to form metal deposits of certain shapes.

Author Keywords

porous silicon; electrodeposition; nickel; indium; silicon-germanium

1. Introduction

Monocrystalline silicon is one of the most advanced artificial materials created by man. Structure and properties of silicon are very well established, and it is generally believed that the prospects for improving its properties are almost entirely exhausted. In this regard, any works aimed at studying the possibilities to create new materials based on silicon with properties that silicon does not normally possess are of significant interest. This paper compiles various results of our research on using porous silicon (PS) formed by electrochemical anodization to create nanocomposites and alloys integrated into a monocrystalline silicon substrate.

The open structure of PS has driven scientists to introduce various "foreign" substances (such as metals and semiconductors) into its pores, in pursuit of creating nanocomposites and hybrid materials with electrophysical properties not akin to monocrystalline silicon [1]. In cases such as these PS plays the role of a "host" material, with the pore-filling material serving as a "guest".

Among various prospective "guests", metals are especially attractive [2]. As part of the present work, we present results on electrodeposition of nickel [3, 4] and indium [5] into PS to fabricate nanocomposites exhibiting specific magnetic and electrical properties. Metal deposits formed inside the pore channels inherit the latter's shapes and sizes.

The second group of prospective "guest" materials are semiconductors. In the current work we present original results on electrochemical deposition of ZnO particles and nanocrystals into PS, causing it to develop noteworthy optical properties [6, 7]. Recently, very attractive results on deposition of germanium into PS were also demonstrated [8]. We discovered that PS filled with Ge can be converted into $Si_{1-x}Ge_x$ alloy films with the use of high-temperature processing [9]. The thickness and composition of silicon-germanium alloys fabricated using this method are determined by the thickness and porosity of the original PS layers employed for their preparation.

As part of the present work, we describe the main formation stages of the aforementioned materials, as well as provide relevant data on their structure, properties and possible applications.

2. Materials and methods

Formation of PS by electrochemical anodization: PS layers were formed by anodizing monocrystalline silicon n-type heavily-doped (0.01 Ohm·cm) wafers in a PTFE electrochemical cell with a platinum counter-electrode at a constant current density of 70 mA/cm^2. As part of this work, we also report novel fabrication regimes of high-porosity nanoporous silicon layers by electrochemical anodization in a C_2H_5OH-based solution containing 1–3% NH_4F and 20–70% H_3PO_4 at a current density of 0.01–0.1 mA/cm^2.

PS Filling with Metals: Electrodeposition of metals into PS was conducted using the same electrochemical cell with the polarity reversed and utilizing bulk samples of corresponding metals as counter-electrodes. Deposition of nickel was performed galvanostatically for 15–80 min at a current density of 3.5 mA/cm^2 using an aqueous solution containing 213 g/l $NiSO_4 \cdot 7H_2O$, 5g/l $NiCl_2 \cdot 6H_2O$, 25 g/l H_3BO_3 and 3 g/l of saccharin.

Similarly, electrodeposition of indium was performed at a constant current density of 0.5 mA/cm^2 for 30 s from an electrolyte containing $In_2(SO_4)_3$, $NaSO_4$ and H_2O in the mass ratio of 6:1:300. All fabricated samples were annealed in vacuum at 200 °C for 15 min to melt the deposited metal particles, which is necessary for their further use as inoculum areas for electrochemical deposition of germanium.

PS Filling with Semiconductors: In order to form silicon-germanium composite materials, germanium was electrochemically deposited into the as-prepared PS samples using an aqueous solution containing 0.05 M GeO_2, 0.5 M K_2SO_4 and 0.1 M $C_4H_6O_4$ (succinic acid) with pH adjusted to 6.5 using NH_4OH. The solution's temperature was maintained at an 85 °C mark under magnetic stirring. The deposition process was carried out for 30 min at a current density of 2 mA/cm^2. The resulting sample was then subjected to rapid thermal processing (RTP) using an Annealsys As-One 100 RTP system at 950 °C over the course of 30 s under argon flow (800 sccm).

For PS/ZnO composite formation, an electrochemical route was also employed by using a highly ordered PS matrix obtained by anodization of n+-type silicon wafers in 9 vol.% aqueous solution of HF in pulsed galvanostatic mode at a current density of 120 mA/cm^2. The thickness of the resulting PS layer was 10 μm. To prevent oxidation of PS side walls during ZnO electrochemical deposition, non-aqueous dimethyl sulfoxide (DMSO) based solution containing 0.03 M $ZnCl_2$ and 0,1 M KCl was used with addition of polyoxyethylene (POE) and H_2O_2.

Structural and elemental analysis: Evaluation of the samples' morphology was conducted using optical microscopy and

scanning electron microscopy (SEM). The latter involved the use of a Hitachi S-4800 SEM also equipped with an EDX spectrograph.

3. Evaluating the structural parameters of PS

The structure of the initial PS matrix is of fundamental importance to the filling factor, as well as to the shape and dimensions of resulting deposits. Porous materials are characterized by macro- and microstructural parameters, with the former including the layer thickness and porosity, and the latter — pore density (number of pores per unit area), pore sizes, distances between pore centers, and thickness of silicon skeleton elements (side walls) between pores. One unique feature of PS lies in the ability to change its structural parameters within a fairly wide range by adjusting electrochemical processing regimes. Figure 1 shows an example cross-section SEM image of a PS sample obtained by anodization at a current density of 70 mA/cm^2 for 30 sec. The thickness of the resulting PS layer is 1.5 μm and the porosity value is 70%. It is characterized by a pore density of $1.4 \cdot 10^{10}$ cm^{-2} and exhibits cylindrical pore shapes with an average diameter of 105 nm, an average distance between pore centers of 85 nm and a pore side wall thickness of 10 nm.

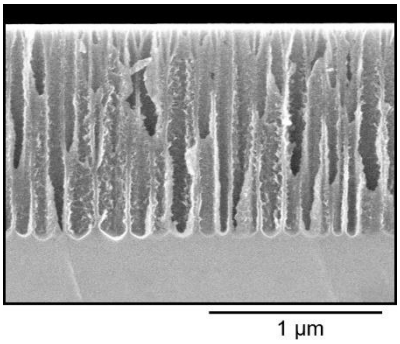

Figure 1. Cross-section SEM image of an initial mesoporous silicon sample used for metal filling

By changing the anodic current density, the aforementioned microstructural parameters can be adjusted. Figure 2 shows the dependence of average pore diameter, distance between pore centers and average side wall thicknesses on the anodic current density. Evidently, changing the current density from 20 mA to 90 mA cm^2 causes the average pore channel diameter to change from 20 to 120 nm, the average distance between pore centers from 30 to 120 nm, and the average pore side wall thickness from 3 to 6 nm. This adjustable morphology is crucial for obtaining differently-shaped pore filaments and has been demonstrated for PS layers with thicknesses ranging from 0.5 μm to as high as 100 μm.

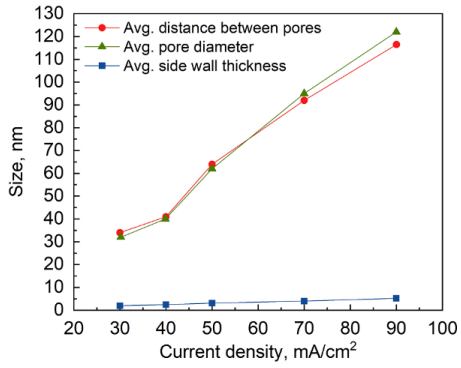

Figure 2. Dependencies of the porous layers' primary microstructural parameters on anodization current density

4. ITO-free LED microdisplays based on thin sponge-like nanoporous silicon layers

CMOS and bipolar technology are today's leading microelectronic approaches. As the most applicable materials in this regard are silicon and aluminum, their integration into display applications remains very desirable. However, being an indirect band gap semiconductor, monocrystalline silicon cannot be used for efficient light emission. A potential breakthrough in this area has occurred in 1990 when quantum effects and room temperature visible luminescence were first demonstrated in PS layers [10]. This feature awoke the researchers´ interest worldwide, and soon the first porous silicon-based light emission diode (avalanche reverse biased Schottky diode) emerged, made possible via silicon nanostructuring [11].

The proposed nanoporous silicon formation regime enables reproducible formation of such layers without the use of hydrofluoric acid, yielding pores with diameters ranging 15 to 20 nm, as illustrated by Figure 3.

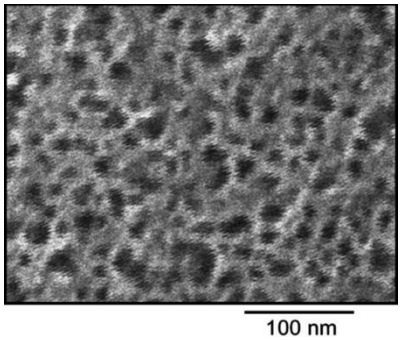

Figure 3. Surface SEM image of nanoporous Si fabricated using 1 wt% NH_4F at a current density of 0.1 mA/cm^2

Afterwards, a Si chip containing a matrix of fast light emitting Schottky diodes, a CMOS row and column drivers can be fabricated. An approach to efficient output light extraction was established using transparent nanostructured conductive Al electrodes (Fig.4). The resulting nanomesh film inherits its electrical conductivity from aluminum, while also exhibiting optical transparency due to the presence of nanoscale pores. Regardless of specific device, the optical transmittance and surface resistance of a nanomesh aluminum film are its most important parameters when used in optoelectronics. Depending on the application, the surface resistance of transparent electrodes can range from 1.0 Ohm/□ to 100 Ohm/□, but optical transparency of at least 80% is required.

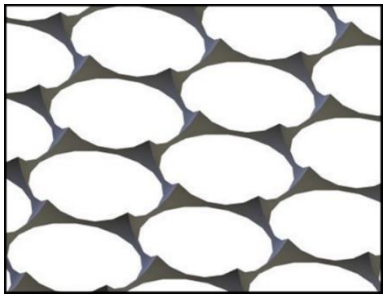

Figure 4. Bird's-eye view of the aluminum nanomesh

The proposed approach can provide an added value thanks to the simple and cheap fabrication process, passive matrix addressing for

microdisplays with full integration of row and column drivers onto a Si chip, high resolution and fabrication yield.

5. PS/Ni composites

Nickel is a metal that possesses striking ferromagnetic properties. Silicon, on the contrary, exhibits almost no magnetic behavior other than extremely low diamagnetic properties. In this regard, forming composite material regions with strong magnetic properties in silicon wafers by PS formation and subsequent pore filling with nickel becomes a promising idea. As an example, we demonstrate the peculiarities of PS-Ni composite formation by filling pore channels of a mesoporous PS layer with nickel. The layer in question was obtained using the same fabrication regimes as the one in Figure 1, but the processing time was increased to obtain a thicker (7.5 μm) layer.

Pore filling was carried out by electrochemical deposition from an aqueous nickel salt solution at a constant current density. The unique feature of this deposition process lies in the ability to obtain different structural forms of nickel deposits by carefully adjusting the working electrode potential. To this end, the potential is recorded using an Ag/AgCl reference electrode tethered as close as possible to the surface of PS via a Luggin capillary.

Figure 3 shows the recorded time dependence of PS potential in relation to the reference electrode. Several characteristic areas with varying potential behavior are observed. The potential values in the electrolyte without external polarization remained nearly constant and fluctuated from -475 to -485 mV. This indicates no noticeable change in reactions on the PS surface, i.e., the surface being stable in this electrolyte. At the moment of current application, the potential increased rapidly to -980 mV, gradually decreasing to -840 mV. After 30 min of deposition, the potential starts to increase slowly again and is stabilized at -950 mV at 55 min without any further change. Stopping the deposition process after 5, 15 and 30 min (curves 1, 2 and 3) led to an immediate decrease in the potential to -375 mV. The same decrease in potential was observed after stopping the process after 60 and 80 min (curves 4 and 5, respectively), but in these cases it took about 30 min for the value to stabilize at -380 mV [4].

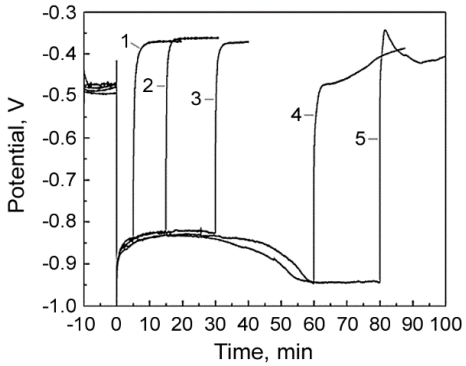

Figure 5. The change in PS potential (vs. Ag/AgCl) with time during nickel electrodeposition. The process was stopped at varying times: (1) – 5 min, (2) – 15 min, (3) – 30 min, (4) – 60 min, (5) – 80 min

The samples obtained at different nickel deposition times (in accordance with Figure 5) were analyzed by SEM. Based on the lowest deposition time sample (Figure 5, line 1), it was found that nucleation and growth of nickel nanoparticles initiates in the lower parts of the porous layer on various side wall protrusions. The diameter of these nanoparticles lies in the range of 40 to 70 nm. Prolonged deposition times (Figure 5, lines 2 and 3 and Figure 6, a) lead to an increase in the linear density of nanoparticles in the central and lower parts of the PS layer. This is attributed to an increase in the number of nanoparticles rather than their size, which remains nearly unchanged.

After an hour-long deposition time, the nanoparticles aggregate into nanofilaments, almost completely filling the pore channels (Figure 5, line 4 and Figure 6, b), which is confirmed by surface potential stabilizing at a value of -950 mV. Any subsequent deposition (Figure 5, line 5) leads to the formation of a continuous nickel film on the sample's surface and is deemed excessive.

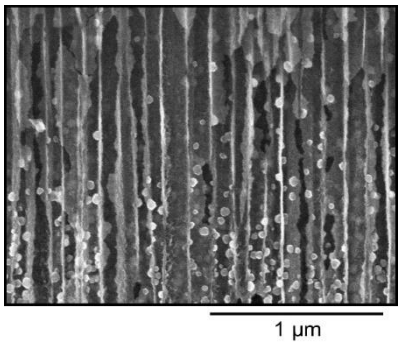

(a) Ni deposited for 30 min

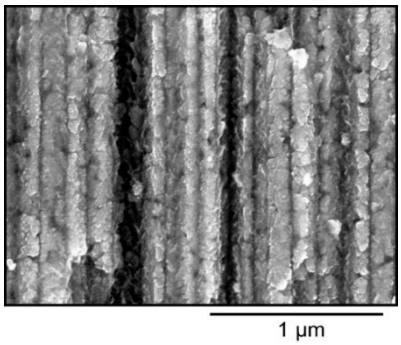

(b) Ni deposited for 60 min

Figure 6. SEM image of PS filled with nickel at different deposition times

All PS samples with nickel deposition times of 5 min and longer possessed ferromagnetic properties [4]. This was confirmed by measuring ferromagnetic resonance at room temperature, as well as the intrinsic magnetization σ and isothermal magnetic hysteresis loops M(H) at varying temperatures T. Samples with deposition times of 30 and 60 min exhibited especially strong ferromagnetic behavior, which is attributed to the presence of nickel nanofilaments. As shown in Figure 7, the specific magnetization and the magnetic moment of Ni atoms, as well as the Curie temperature values are smaller for the sample with non-continuous Ni nanowires with respect to those reported for bulk Ni.

Noteworthy results were obtained when studying an array of nickel nanowires embedded in a matrix of porous silicon using the ferromagnetic resonance method, making it possible to determine the anisotropy features of the samples. It was found that for PS samples with a porosity of 50% (formed at 50 mA/cm^2), magnetic anisotropy of the light axis type along the nickel nanowires was observed. For samples with a porosity of 80% (formed at 90

mA/cm^2), anisotropy of the light plane type was characteristic [5].

The data obtained for arrays of oriented nickel nanowires in PS are of interest both from the point of view of studying magnetic ordering in heterogeneous systems and from the applied point of view, as they can be deemed promising materials for the creation of sensors and magnetic storage devices.

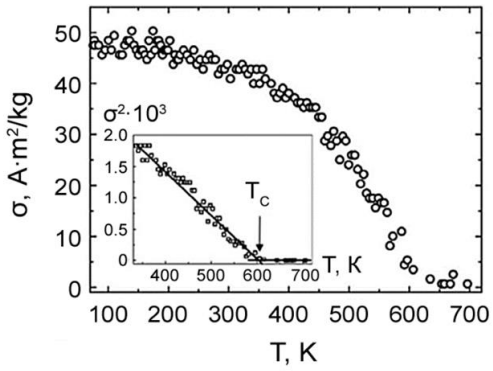

Figure 7. Temperature dependence of specific magnetization σ for PS template after 15 minutes of Ni deposition. Inset: σ^2 versus temperature dependence

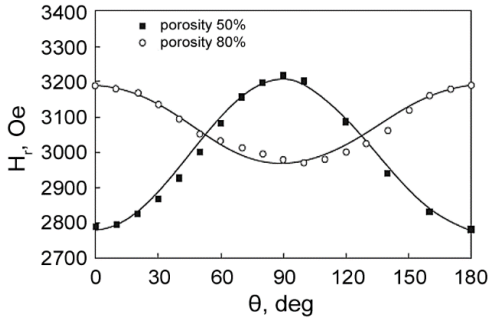

Figure 8. The dependence of resonance field strength H on the angle θ between the constant magnetic field direction and the normal to the surface of PS samples with two different porosities

6. PS/In composites

Historically, indium deposition on PS was first studied as a means to providing electrical contacts to porous layers and measuring their electrical characteristics. Similarly to nickel, indium particle deposition was also explored as a way to greatly improve photoluminescent properties of PS. Lastly, as part of our recent work, indium was viewed as a precursor material for subsequent ec-LLS growth of germanium crystals within the pores of PS. In this process indium particles simultaneously act as microscopic cathodes and a growth medium for crystalline germanium. However, to maximize its effectiveness for this application, indium should be deposited at the very bottoms of the pore channels, ensuring complete pore filling with germanium.

In contrast to nickel deposition, selective deposition of indium proved to be a difficult task. Localizing indium deposits at pore bottoms proved to be practically impossible without additional preparation stages. The main reason for this lies in the state of the silicon side wall surface, which is terminated by hydrogen atoms and contains a very large number of structural defects and doping atoms, causing indium deposition to mainly occur along the sidewalls and on the surface of the PS layer. We have shown that oxidation of PS in an air atmosphere at 300 °C or in an aqueous HNO_3 (50 vol. %) can drastically the pore filling factor when electrodepositing indium from aqueous solutions [5]. Due to PS oxidation primarily occurring in its topmost parts, indium concentration shifts down from subsurface areas as a result of preliminary PS oxidation. The greatest effect is shown in the case of chemical oxidation in HNO_3 solution, at which a significant concentrations inside the lower half of the pores was achieved, as illustrated by Figure 9.

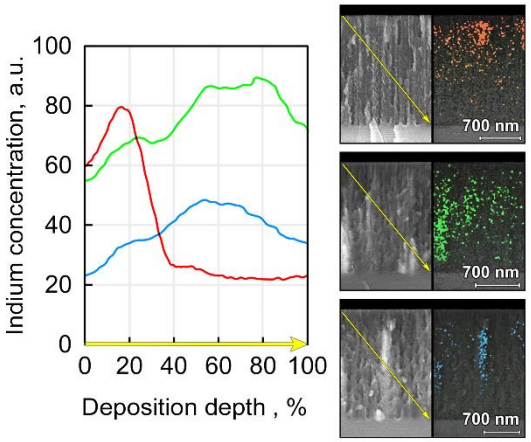

Figure 9. SEM images and corresponding EDX maps showing indium distribution on the lateral spall of PS samples with deposited indium: (red) unoxidized, (blue) thermally oxidized and (green) chemically oxidized

7. PS/Ge composites and Si_xGe_{1-x} alloys

To form PS/Ge composite structures, germanium must be deposited into the pore channels. Approaches to electrochemical deposition of germanium on conductors and "flat" semiconductors have long been established; however, they are largely inapplicable to PS electrodes for a number of reasons, mainly associated with its large surface area which causes high activity and unwanted etching in most known solutions. As mentioned in Section 5, this can be solved by employing the ec-LLS technique, which involves forming preliminary indium deposits in the pore bottoms followed by germanium electrodeposition from a GeO_2-containing solution. Figure 10 shows a cross-section SEM image of a PS sample analogous to the one presented in Figure 1 with its pore channels electrochemically filled with germanium. Notably, this method of pore filling is sufficiently homogeneous. Based on the accompanying EDX concentration profile, it can be concluded that silicon and germanium are present in the layer in a roughly 1:4 ratio.

By subjecting these silicon-germanium composites to high-temperature thermal processing, a thin layer of a silicon-germanium alloy is formed, as shown in Figure 11. Based on Raman spectroscopy and EDX data, its composition is estimated to be $Si_{0.28}Ge_{0.72}$.

It is important to note that the resulting alloy's composition directly corresponds to the ratio of silicon and germanium in the initial composite, which in turn is directly tied to the porosity value dictated by the anodization regimes. Similarly, the alloy's thickness corresponds to that of the initial PS layer, but is reduced slightly due to the presence of unfilled gaps [9].

The alloys exhibited good thermoelectric parameters, making them

well suitable for use in high-temperature thermoelectric converters, as well as photodetectors.

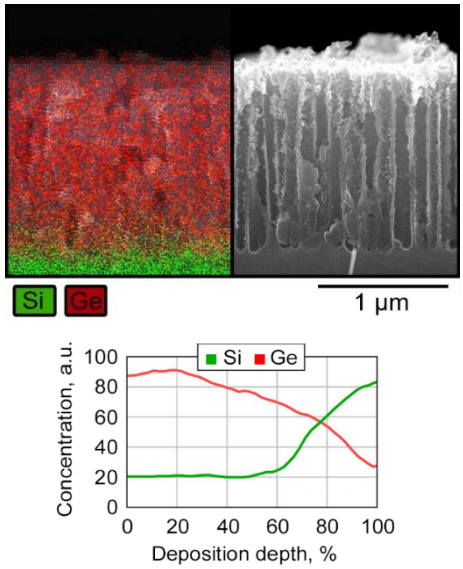

Figure 10. Cross-section SEM image, EDX map and EDX concentration profile of a PS sample filled with germanium

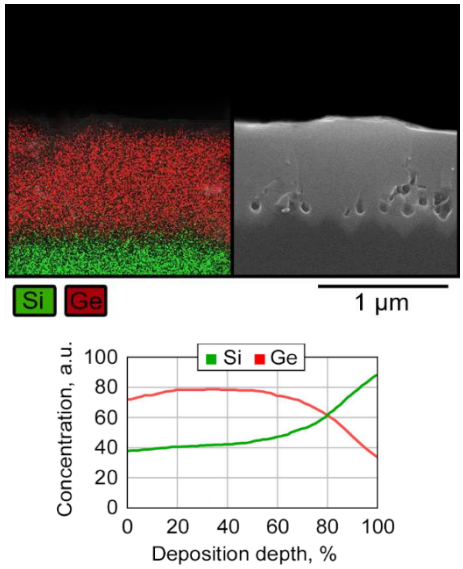

Figure 11. Cross-section SEM image, EDX map and EDX concentration profile of a PS sample filled with germanium and subsequently annealed for alloy formation

8. PS/ZnO composites

ZnO is a direct band-gap semiconductor with good light emitting capabilities. Its bandgap width of 3.37 eV at 300 K makes it suitable for use in UV and visible range devices [12, 13]. As is the case with silicon, the light emission efficiency of ZnO can be considerably improved by nanostructuring. One of the ways to obtain an array of ZnO nanostructures is to use ordered matrices of PS, with their pore diameters determining the sizes of resulting ZnO structures. It was shown that such PS/ZnO nanocomposite materials can be used as white light sources [12], as well as gas sensors [13].

Using current density of 0.3 mA/cm^2 and deposition times ranging from 60 to 240 min different pore filling factors were achieved (Figure 12), as determined by gravimetry and optical spectroscopy.

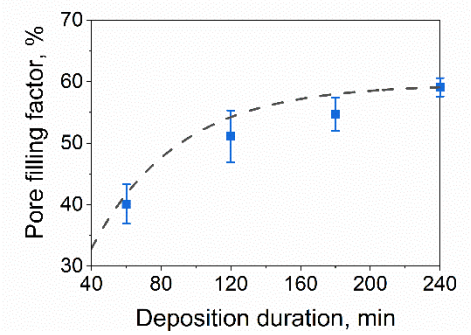

Figure 12. Pore filling factor for PS with ZnO particles deposited with different process duration

A pore filling factor around 60 % is achieved. Any further increase is inhibited by ZnO crystals accumulating at pore entrances and preventing electrolyte access into the channels. As such, any subsequent ZnO reduction occurs only the surface of PS. The growing concentration of ZnO crystal inside the porous structure with increasing deposition duration is also confirmed by cross-section SEM images of obtained PS/ZnO composite (Figure 13).

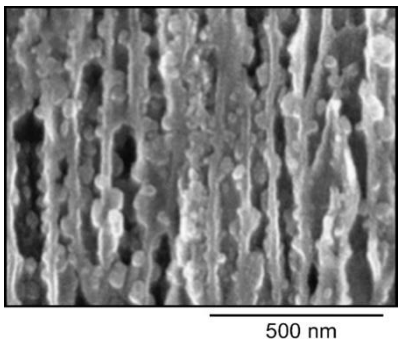

(a) ZnO deposited for 120 min

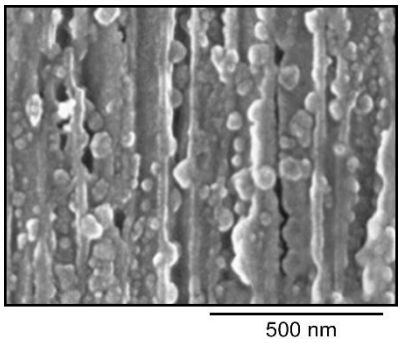

(a) ZnO deposited for 240 min

Figure 13. Cross-section SEM images showing central parts of a PS/ZnO composite obtained at current density of 0.3 mA/cm^2 at varying ZnO deposition times

The average equivalent size of ZnO particles formed inside mesoporous silicon linearly increases with deposition current density (Figure 14).

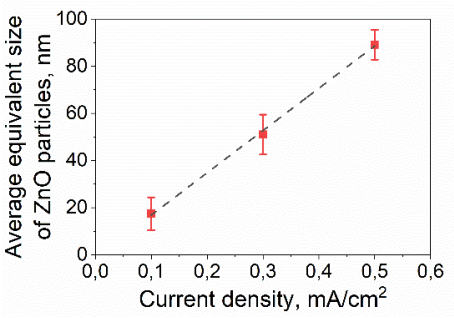

Figure 14. Dependence of average ZnO particle size on deposition current density

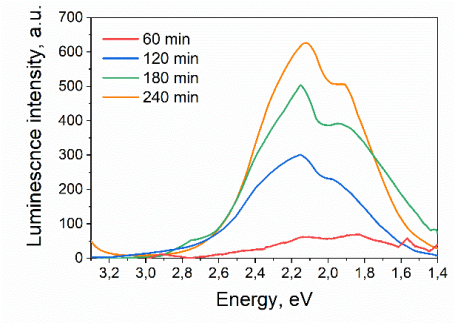

Figure 15. Luminescence spectra of PS/ZnO composites obtained at different process duration

The resulting PS/ZnO composites demonstrate visible range luminescence, with the emitted light intensity directly determined by deposition duration (Figure 15). As such, the obtained PS/ZnO composite materials are suitable for use in visible light sources and display devices.

9. Conclusions

Based on SEM, EDX, magnetic and optical measurements, it can be concluded that a variety of structures based on PS can be potentially applied to the production of displays and/or other optical devices. This is directly enabled by PS's photoluminescence stemming from its nanostructured morphology, as well as from the ability to electrochemically fill or decorate the pores with other materials, which additionally enhance its already noteworthy capabilities.

10. Acknowledgements

We would like to thank D. Zhigulin (State Center "Belmicroanalysis", Affiliate Research & Design Center "Belmicrosystems", JSC "INTEGRAL", Minsk, Belarus) for conducting SEM and EDX analyses of the experimental samples.

The results listed in this work were acquired under financial support of the Belarusian Republican Foundation for Fundamental Research (project № T23M-040), the master student grants provided by the Ministry of Education of Belarus (projects № 24-3163M and 24-3165M), the Russian Science Foundation (project № 20-19-00720, https://rscf.ru/project/20-19-00720/), State Programs of Scientific Research of Belarus «Physical Materials Science, New Materials and Technologies» (project № 2.25) and «Convergence 2025» (project № 3.02.5).

11. References

1. Chubenko E, Redko S, Dolgiy A, Bandarenka H, Prischepa S, Bondarenko V. Porous Silicon as Host and Template Material for Composites and Hybrid Materials. In: Korotchenkov G. (ed.) *Porous Silicon: From Formation to Applications.* CRC Press, Taylor and Francis Group, USA; 2016. p. 181–205.
2. Bandarenka H, Dolgiy A, Chubenko E, Redko S, Girel K, Prischepa S, et al. Nanostructured Metal Films Formed onto Porous Silicon Template. *Journal of Nano Research*. 2016;39: 235–255. doi: 10.4028/www.scientific.net/JNanoR.39.235
3. Rusetskiy M, Kazutchits N, Baev V, Dolgiy A, Bondarenko V. Magnetic anisotropy of Ni-nanowires massive in porous silicon. *Technical Physics Letters.* 2011;37(9): 1–4. doi:10.1134/S1063785011050142.
4. Prischepa S, Dolgiy A, Bandarenka H, et al. Synthesis and properties of Ni nanowires in porous silicon templates. In: Wilson L. (ed.). *Nanowires*. Nova Science Publishers, Inc.; 2014. p. 89–129.
5. Grevtsov N, Chubenko E, Bondarenko V, Gavrilin I., Dronov A., Gavrilov S. Electrochemical Deposition of Indium onto Oxidized and Unoxidized Porous Silicon. *Thin Solid Films.* 2021;734: 138860. doi:10.1016/j.tsf.2021.138860.
6. Sherstnyov A, Redko S, Petrovich V, Chubenko E. Electrochemical deposition of zinc oxide nanostructures into porous silicon template. Proc. International Conference Nanomeeting-2015, Minsk, Belarus. 2015. p. 276–279.
7. A.I. Sherstnyov A, Chubenko E, Redko S, Petrovich V, Pilipenko V, Bondarenko V. Formation of nanocomposite materials based on porous silicon and zinc oxide by electrochemical method. *Doklady BGUIR*, 2016; 95(1): 82–88. (In Russ.).
8. Grevtsov N, Chubenko E, Bondarenko V, Gavrilin I, Dronov A, Gavrilov S. Germanium electrodeposition into porous silicon for silicon-germanium alloying. *Materialia*. 2022;26: 101558. doi: 10.1016/j.mtla.2022.101558.
9. Grevtsov N, Chubenko E, Bondarenko V, Gavrilin I, Dronov A, Gavrilov S, et al. Composition adjustable silicon-germanium alloy films based on porous silicon matrices. *Materials Today Communications.* 2024;38: 107886. doi: 10.1016/j.mtcomm.2023.107886.
10. Canham L. Silicon Quantum Wire Array Fabrication by Electrochemical and Chemical Dissolution of Wafers. *Applied Physics Letters.* 1990;57: 1046–1048. doi: 10.1063/1.103561.
11. Jaguiro P, Katsuba P, Lazarouk S, Farmer M, Smirnov A. Si-based emissive microdisplays. *Physica E: Low-dimensional Systems and Nanostructures* 2009;41: 927–930. doi: 10.1016/j.physe.2008.08.002.
12. Özgür Ü, Alivov Ya, Liu C, Teke A, Reshchikov M, Doğan S. A Comprehensive Review of ZnO Materials and Devices. *Applied Physics Reviews.* 2005;98: 041301. doi: 10.1063/1.1992666.
13. Qiao Q, Li B, Shan C, Liu J, Yu J, Xie X. Light-emitting diodes fabricated from small-size ZnO quantum dots. *Materials Letters.* 2012; 74: 104–106. doi: 10.1016/j.matlet.2012.01.048.